THE EFFECT OF CLAHE TO LOG-GABOR FILTER UN-SHARP MASK FOR FINGER VEIN IMAGE ENHANCEMENT AND CLASSIFICATION

Amir Hajian, Dzati Athiar Ramli* and Shazeeda
School of Electrical & Electronic Engineering, Universiti Sains Malaysia, Nibong Tebal, Penang 14300, Malaysia.
amirhajian85@gmail.com, dzati@usm.my, shaju9009@gmail.com

ABSTRACT. *Finger vein biometrics have been considered as one of the promising authentication methods nowadays. However, the main problems of finger vein image are low contrast and poor sharpness qualities because the image is normally captured under uneven illumination. The use of Classical Un-sharp Mask (CUM) is capable to modify the contrast and sharpness of finger vein image, however, its halo effect and excessive sensitivity to noise are the inevitable consequences. Therefore, this paper proposes a novel algorithm to enhance contrast and sharpness qualities of finger vein image by integrating Contrast Limited Adaptive Histogram Equalization (CLAHE) technique with a modified version of Un-sharp Mask (MUM) which is based on the Log-Gabor filter technique. The significance of this proposed algorithm is evaluated by quantifying the improvement of vein detection through the Modified Repeated Line Tracking (MRLT) feature extraction. For the performance assessment, the SDUMLA finger vein database containing 3816 finger images is utilized. The experimental results revealed that the tiny veins became significantly more pronounced and sharp with 6.28% Equal Error Rates (EER) performance compared to 9.22% and 16.66% EER of MUM and baseline performances, respectively. Thus, the findings of the current study demonstrate the significance of the proposed enhancement algorithm.*

Key Words: *Finger vein, Contrast Limited Adaptive Histogram Equalization, Modified version of Unsharp Mask.*

1. INTRODUCTION

The growth of data science and information system leads biometric technology to become one of the best solutions to secure the automated authentication and identification process, especially for border control and internet banking system [1, 2]. One of the excellent characteristics of finger vein compared to fingerprint [2], iris [3], voice [4] and face [5], is that it is a sort of internal and invisible modality which is located underneath the finger skin and unseen to human naked eyes. Therefore, the risk of replicating the vein pattern by hackers is more challenging compared to the other external and visible biometric traits [6]. Apart from that, as every person has generally ten fingers thus if an unforeseen incident happens to any of the fingers, other fingers are available for replacement during the authentication and identification process [7].

Generally, a typical biometric system based on finger vein modality has four important modules. The first module is the finger vein data collection process, followed by pre-processing of the finger vein sample, finger vein feature extraction process, and finally, pattern matching for the authentication or identification [8], [9]. Figure 1 illustrates the four modules in the finger vein authentication system.

Figure 1: Block diagram of the finger vein recognition system

For the data acquisition device, near-infrared (NIR) light (760-850nm) is normally used for visualizing the finger vasculature. When the NIR light penetrates into the finger, the light is absorbed by the Deoxyhaemoglobin in venous blood and the vascular pattern is ready to be captured by the CCD sensor [10]. However, due to uneven illumination and different thickness of the fingers, the captured images contain irregular shadows that mixed up with the veins and these images are normally referred to as low contrast and poor sharpness images [11]. Therefore, a pre-processing stage will play an important role in ensuring the significant preservation of all essential vein information, as the feature extraction process will affect the quality of the extracted features of the finger vein. The low performance of the feature extraction technique will certainly affect the final classification output. Robust extraction of vein features should contain all the minute details of tiny veins which lead to the high accuracy of the recognition system. In the pre-processing stage, the Region of Interest (ROI) is first detected and followed by image enhancement procedures [12].

So far, various image enhancement techniques have been implemented so as to improve the quality of finger vein features [13, 14, 15, 16, 17]. Yang *et al.*, [13], used the even-symmetric Gabor filter bank with eight orientations to exploit the vein information from the ROI. An image containing the integrated finger vascular was then generated by the image reconstruction procedure. However, since this method enhances the low-contrast areas of the ROI more than the other parts, the small details of vein from the low contrast area which carries important vein information are also eradicated by this enhancement process. Therefore, in order to solve this problem, Yang *et al.*,[14], then utilized a family of Gabor wavelets to enhance the sharpness of the low-contrast vascular region and the circular Gabor filter was used for reconstruction. However, the drawback of this approach is the halo effect which appears in the resulting image. Due to this, Yang *et al.*, [15], then used a new anisotropic diffusion method with a standard deviation map constraint to estimate the local background illumination. The non-scatter transmission maps were then estimated by the gamma correction. However, the processing speed of this approach is significantly slow. A multi-scale matched filter technique was also applied in a study by Gupta and Gupta, [17], however, this technique is extremely sensitive to noise. In another research, Banerjee et al., [16], combined the fuzzy contrast enhancement technique with the CLAHE operator

to enhance the sharpness and contrast of the finger vein image for the authentication system. Although this technique enhances the contrast of the finger vein image to some extent, yet the enhancement of sharpness of the image was an undesirable performance in terms of solving the greyness ambiguity of the input image.

From the previous study, it can be observed that several methods have been proposed by the researchers on pre-processing so as to solve the low contrast and poor sharpness quality of the images. However, it is quite challenging to improve the contrast and sharpness of the images simultaneously. Therefore, the main focus of the current study was to improve the contrast and sharpness qualities of the images.

The remainder of this paper is organized as follows. Section 2 explains the details of the methodology, including the proposed image enhancement algorithm and followed by results and discussion in Section 3. Finally, the conclusion is given in Section 4.

2. Methodology

This section discusses the steps in developing the finger vein authentication system. The proposed enhancement algorithm which is the backbone of this study is comprehensively explained in section 2.3.

2.1 Data Collection

For the data acquisition device, near-infrared (NIR) light (760-850 nm) is normally used for visualizing the finger vasculature. When the NIR light penetrates into the finger, the light is absorbed by the Deoxyhaemoglobin in venous blood and then the vascular pattern is ready to be captured by the CCD sensor [10]. In this research, the SDUML-HMT finger vein database, consists of 106 subjects of male and female, is used for the experimental data [18]. The ring finger, middle finger, and index finger of both hands were stored in this database and the capturing process is repeated 6 times for each of these fingers. In total, the database comprises of 3,816 finger vein image samples, each with 320×240 pixels resolution in BMP file format and with a total size of 0.85G Bytes. A computer with Intel Core i5, 1.6 GHz, and 4GB RAM is used to execute the programming for this study.

2.2 Region of Interest (ROI) Detection

The first step in the pre-processing stage is to detect the borders of the finger. The identification and highlighting specifically the finger area from its background are called ROI detection. The left and the right boundaries of finger image in the horizontal direction are determined by X_L and X_R, respectively. In this study, the values of the left side, X_L, and right side, X_R of the image with 320×240 pixels are experimentally defined as 10 and 38 pixels, respectively.

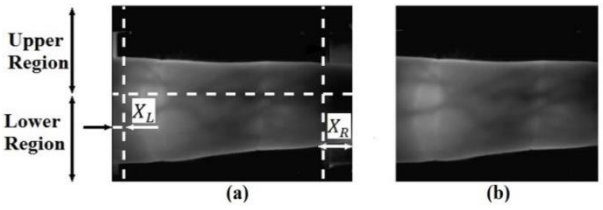

Figure 2: Detection of left and right boundaries (a): Original image and, (b): Output image after detection.

Figure 2 represents the left and right side boundaries.

The finger vein image consists of a finger part with higher grey-level value, surrounded by a background with lower grey-level value as shown in Figure 2. The upper and lower boundaries of finger regions are detected by using two 4×20 masks, as shown in Figure 3.

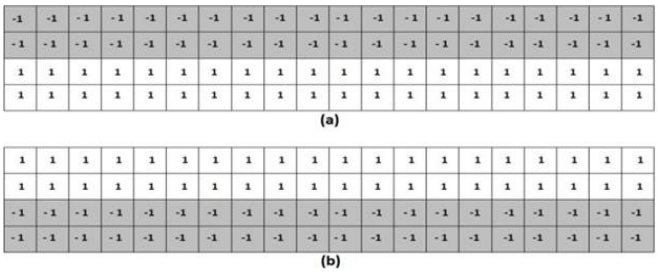

Figure 3: The 4 x 20 masks for ROI detection (a): Mask for upper boundary (b): Mask for the lower boundary

Since the background of the image has a lower grey-level value compared to the finger region, therefore the pixel values of finger boundaries in upper and lower parts of the finger became maximum, and the borders of the finger were detected. Figure 4 demonstrates the upper and lower boundaries that were detected as the ROI.

Figure 4: Upper and lower boundary detection of finger image: (a) the original image, (b) binary image (c) detected upper and lower finger edges

In contrast to other ROI detection methods, the upper and lower boundaries of the finger are not detached from the image [19, 20, 21]. In this study, the detected boundaries are used in the feature extraction stage, whereas the vein detection was performed based on the pixel values inside the boundaries.

2.3 The proposed enhancement algorithm

The advantage of using Classical Un-Sharp Mask (CUM) and its variation for sharpness and contrast enhancement in medical image has been evaluated in a study by Gurpreet (2013) [22]. For simplicity, the output of Classical Un-Sharp Mask algorithm, v can be given as $y + \gamma(d)$ as in equation (1) below.

$$v = y + \gamma(d) \qquad (1)$$

Here, y and γ refer to the result of a linear low-pass filter and gain which is a real scaling factor. Here, d is obtained by subtracting the input image signal, x with the result of a linear low-pass filter, y. In order to increase the sharpness, the signal, d is amplified by γ ($\gamma > 1$). However, this process amplifies the noise and enhance the under-shoots and over-shoots in the areas of sharp edges due to the smoothing process. In one of the studies [22], a filter that ideally enhances the details of the image without being

sensitive to noise and without smoothing the sharp edges was investigated using a modified version of CUM on the medical images.

Subsequently, Hajian & Ramli, [23], implemented the modified version of CUM called as a modified un-sharp mask (MUM) by replacing the low pass filter with a log-Gabor filter to enhance the contrast and sharpness of finger vein image. Although this method manages to visualize the smaller details of vein vasculature, yet it suffers from uneven illumination on the resulted image as shown in Figure 5. This is due to the sharper regions of finger image which is over enhanced compared to the regions of the lower dynamic range and this leads to the appearance of an unpleasant halo effect. Halo is unwilling bands of light that appears when the high-contrast edges, which are located in the higher grey-scale pixel regions of the image, are over enhanced [23].

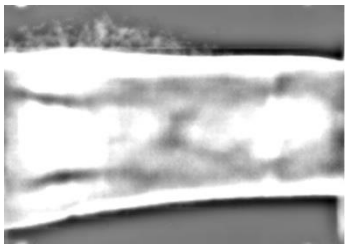

Figure 5: MUM algorithm and the unfavorable halo effect.

According to the generalized linear system, the signal is decomposed into two parts. One part is the signal that fits into the particular model and another is the residual part [24, 25, 26]. By referring to equation (1), the filtering output of y is considered as the part of the image that fits into this model while d is defined as the detail signal or residual signal. Obviously, this mathematical model shows that the part of the image that needs to be sharpened is the residual part, while, another part executes the contrast enhancement, which can be done by executing certain processing algorithms such as histogram equalization.

Since the MRLT algorithm operates based on the cross-sectional profile of the image which can eliminate the halo effect, noise plays an important role in getting the most appropriate features from the tiny vein pattern. Therefore, this paper proposes an image enhancement algorithm that

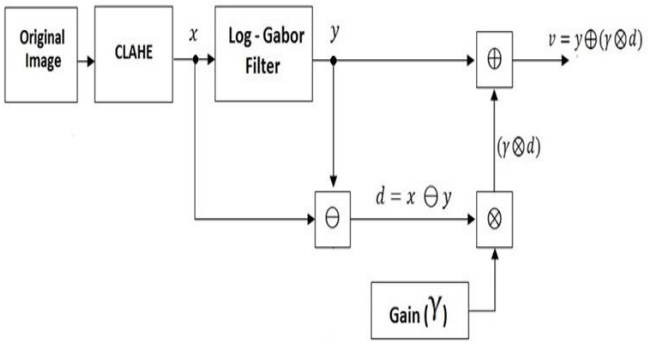

Figure 6: Block diagram of image modification in the pre-processing stage of MRLT algorithm

can improve the MRLT feature extraction by combining Contrast Limited Adaptive Histogram (CLAHE) and a modified version of Un-sharp Mask (MUM) which is based on Log-Gabor filter. These two techniques seem to complement each other in solving the low contrast and poor sharpness of tiny vein images specifically for the cross-sectional profile image as in the case of the MRLT algorithm.

Hence, the overall modification on image enhancement conducted in this study was the use of CLAHE and Log Gabor filter during the pre-processing phase. The overview of the study is shown in Figures 6 below.

2.3 (a) Contrast Limited Adaptive Histogram Equalization (CLAHE)

This method operates based on a local enhancement approach. The image is first partitioned into non-overlapping blocks with equal size regions called tiles [27, 28]. Each non-overlapping tile has size $(M \times N)$ and it is categorized into three different types of tiles i.e. corner region (CR), border region (BR), and inner region (IR) as shown in Figure 7.

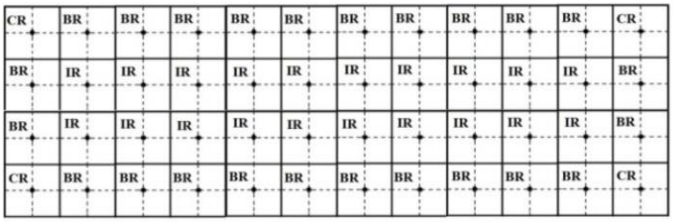

Figure 7: The organization of tiles in finger image

CR regions are the 4 tiles at the image's corner, BR regions are the tiles of the border of the image and the rest of the tiles are considered as IR regions. As the size of ROI is 272×240 pixels, the image is divided into 1,020 tiles in which each tile is composed of 8×8 pixels size.

The histogram of each tile is calculated using Cumulative Density Function (CDF) with the help of the following equation:

$$f_{i,j}(n) = \frac{(N-1)}{M} \cdot \sum_{k=0}^{n} h_{i,j}(k) \qquad (2)$$

where M and N are considered as the number of pixels for each tile, $h_{i,j}(k)$ is the histogram of pixel k and $n = 0, 1, 2, \ldots, N-1$.

The clip limit value (β) is determined by the following equation:

$$\beta = \frac{M}{N}\left(1 + \frac{\alpha}{100}(S_{max} - 1)\right) \qquad (3)$$

where α is the clip factor and it can be between 0 and 100. The maximum allowable is S_{max} that can be between 1 and S_{max}, and M and N are the tile dimensions. The histogram of each independent tile is modified based on the obtained clip limit. In other words, the histogram of each tile that exceeds the value of the clip limit is limited to β and retains the histograms that are lesser than or equal to $\beta = 0.01$. This process is repeated until the entire histogram values of tiles become lesser than or equal to the clip limit value.

After clipping and redistribution of histograms, the calculation of new pixel values with the mapping function is done based on redistributed histograms. Three different mapping functions are used for mapping new pixels values according to three different types of tiles.

Mappings of te four nearest neighbors are used for IR type tiles in order to determine the mapping of each quadrant in the region. Figure 8 demonstrates the specified pixel in quadrant 1 of (i,j) region. Depend on vertical and horizontal distances of this pixel from the centers of $(i,j),(i-1,j),(i-1,j-1)$, and $(i,j-1)$, the new value for this pixel is calculated using the following equation.

$$p_{new} = \frac{s}{r+s}\left(\frac{y}{x+y} f_{i-1,j-1}(p_{old}) + \frac{x}{x+y} f_{i,j-1}(p_{old})\right) + \frac{r}{r+s}\left(\frac{y}{x+y} f_{i-1,j}(p_{old}) + \frac{x}{x+y} f_{i,j}(p_{old})\right) \quad (4)$$

Where $f_{i,j}(\cdot)$ is a cumulative distribution function, and $x, y, s,$ and r are the specified distances as shown in Figure 8. The new pixel values of other quadrates (2, 3, 4) are computed the same way.

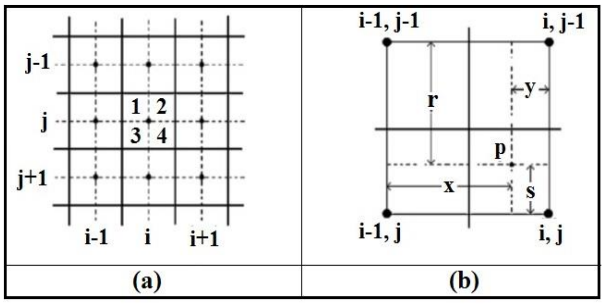

Figure 8: The IR tile. (a) The bordering regions. (b) The center, P and the four nearest regions

Subsequently, the condition of BR type tiles is demonstrated in Figure 9. The calculation of new pixel value in quadrant 1 or 3 is similar to that of the IR type, while the calculation of new pixel value for quadrant 2 or 4 is calculated as follows:

$$p_{new} = \frac{s}{r+s} f_{i,j-1}(p_{old}) + \frac{r}{r+s} f_{i.j}(p_{old}) \quad (5)$$

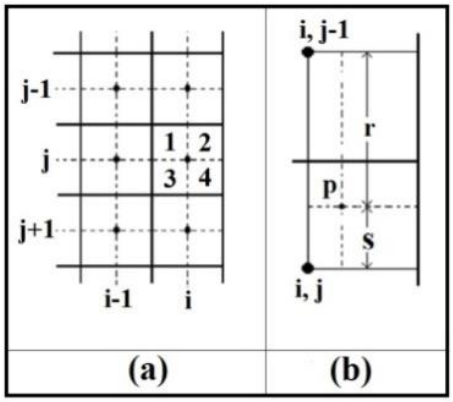

Figure 9: The BR tile. (a) The bordering regions. (b) The center, P and the four nearest regions

Finally, Figure 10 shows the condition of a CR type tile. The neighborhood situation of quadrants 2 and 3 are similar to BR type tile and the neighboring organization of quadrant 4 is similar to IR type tile. Therefore, the new pixel values of these quadrants in the corner position are computed with BR and IR equations. The new pixel value of pixel p in quadrant 1 of (i,j) in corner tile is computed by the following equation,

$$p_{new} = f_{i.j}(p_{old}) \quad (6)$$

Figure 11 demonstrates the contrast enhancement of finger images before and after implementing the CLAHE method.

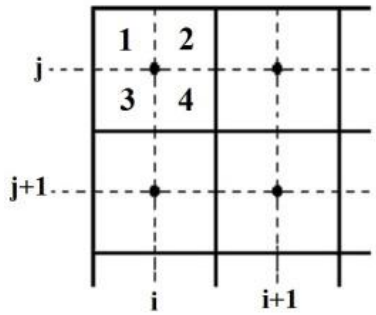

Figure 10: The CR tile

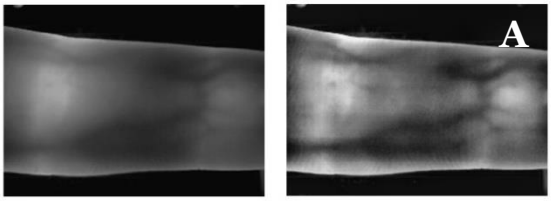

Figure 11: Original image (A) and CLAHE enhancement (B), respectively

2.3 (b) Log Gabor filter design

The Log-Gabor filter is constructed in terms of two main components, radial, and angular components. The frequency band of the filter is controlled by the radial component and orientation directions of the filter are controlled by the angular component. In order to improve the contrast of the image in the Log-Gabor filter, both the radial and the angular components are multiplied together. The transfer function of the Log-Gabor filter is given by the equation (7) below

$$G_{pk} = G(\rho,\theta,p,k) = \exp\left(-\frac{1}{2}\left(\frac{\rho-\rho_k}{\sigma_\rho}\right)^2\right)\exp\left(-\frac{1}{2}\left(\frac{\theta-\theta_{pk}}{\sigma_\theta}\right)^2\right) \quad (7)$$

where (ρ,θ) represents the log-polar coordinates (log_2 scale demonstrates the filters organized in octave scale), p and k are orientation and scale, respectively. The pairs $(\sigma_\rho,\sigma_\theta)$ correspond to angular and radial bandwidths.

The filter bandwidth is set by a parameter which is the ratio of standard deviation in the log frequency domain to the center frequency of the filter. The value of 0.65 for this

parameter obtains a bandwidth of roughly 2 octaves. The maximum and minimum frequencies of the Log-Gabor filter are determined by the wavelength of the smallest scale and the wavelength of the larger scale of the filter, respectively. Although the smallest value of wavelength is the Nyquist wavelength of 2 pixels; but for restricting the aliasing problem; the minimum value is set to 3 pixels in Log-Gabor design in order to obtain the maximum frequency. The minimum frequency implicitly defined by

$$Minimum\ Frequency = {}^{1}/_{Maximum\ waveleng}\,th \quad (8)$$

Small wavelengths lead to the high frequencies at the corner of FFT and make FFT with uneven coverage. The uneven coverage may depress the normalization process during phase congruency computation. In order to solve this problem and produce FFT with uniform coverage in all directions, a low-pass filter (as large as possible) is multiplied with the filters.

The angular component of the Log-Gabor filter controls the resolution of orientation information. The angular interval between filter orientations of Log-Gabor is fixed by the number of filter orientations. In this study, the optimum filter orientation was chosen by analyzing 6 different orientations of the filter. By taking the inverse Fourier Transform of the filter, the real part of the result (even-symmetric component) and the imaginary part of the result (odd-symmetric component) are obtained. Figure 12 (a) and (c) show the even-symmetric component and Figure 12 (b) and (d) demonstrated the odd-symmetric component of the filter.

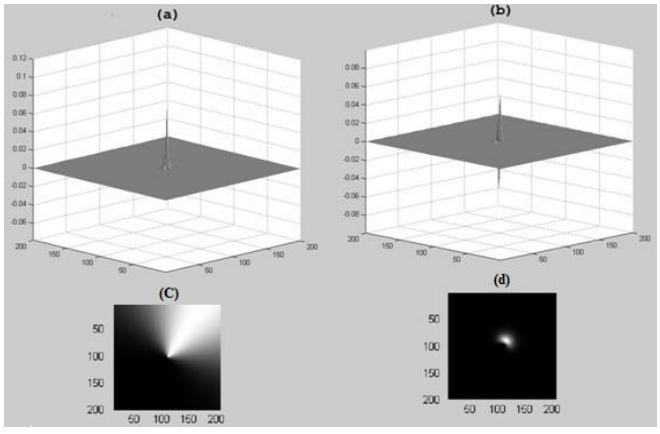

Figure 12: Log-Gabor Filter design: (a) and (c) are the even-symmetric component while (b) and (d) are the odd-symmetric component of the filter.

2.3 (c) Summary of the proposed image enhancement algorithm

The architecture of the overall method proposed for image enhancement as presented in Figure 6 is summarised into Algorithms 1, 2, 3 as given below. The effect of finger vein image enhancement to the feature extraction stage will be discussed in the next part of the paper.

Algorithm 1: ROI detection

Input: (a) $Input\ image = [320 \times 192]$
(b) $x_L = 10$ and $x_R = 282$
(c) $mask\_height = 4$, $mask\_width = 20$

Output: (a) *The detected ROI image* $= [272 \times 192]$

Algorithm:

Step1: Determine the left and right boundaries of the input image

The value of the left boundary (x_L) set to 10 pixels and the value of the right boundary (x_R) set to 282 pixel

The new x value for the input image is considered to determine by the formula $x = x_L \cap x_R$

Step2: Detect the upper and lower boundaries of the input finger

- The height of the input image is divided into the same size, upper and lower regions.
- Construct masks by filtering the upper half and the lower half of the images.
- Filter both halves of the image using these masks
- Determine the pixels which are in the upper and lower borders of the resulting binary image.

2.4 Feature Extraction by Modified Repeated Line Tracking (MRLT)

Feature extraction is one of the important processes in a finger vein authentication system. It transforms the raw input data into a set of salient information, namely, features. It involves a data selection process and finally facilitates the process of dimension reduction. There are various algorithms and filters used in precisely extracting the vein features from the raw finger image. These methods are classified into three main categories which are vein pattern-base [29], dimensionality reduction-based [30], and local binary-base [31] methods. Modified Repeated Line Tracking (MRLT), the algorithm that was used in this study, belongs to the vein pattern-base category [32]. This algorithm operates based on a vein image cross-sectional profile and it has an ability to extract the salient information from the vein images.

The minutiae algorithm, Repeated Line Tracking (RLT), developed by Miura and Nagasaka, [11], to resolve the problem of precise detection of finger vascular pattern from the dark and shadowy image, whereas, MRLT method is the improved version of the RLT algorithm and it detects the vein pattern according to cross-section profile of finger image [23, 32]. The cross-sectional profile of the vein has a valley shape and the depth of the valley indicates the pixel with the darkest intensity value as shown in Figure 13 below.

Algorithm 2: CLAHE

Input:	$ROI\ detected\ image = [272 \times 192]$
Output:	*Histogram equalization according to clip limit for all non-overlap tiles*

Algorithm:

Step1: Partitioned the image into non-overlap tiles [M × N]
The image [272×192] is divided into 816 tiles in which each tile has a 4×4 pixel size

Step2: Histogram equalization
The histogram equalization of each tile is calculated by the Equation (2)

Step3: Calculation of the clip limit value and mapping new value for each pixel
The clip limit of each tile (β) is calculated by the Equation (3)
The new value for each pixel is calculated according to the type of each tile by the Equation (4), Equation (5), and Equation (6).

Algorithm 3: log Gabor filter

Input: (a) $CLAHE\ image\ x = [272 \times 192]$
(b) *Log-Gabor filter with* $p = 6$ *(filter orientations) and* k *=5 (filter scales)*
(c) $\gamma = 2$

Output: (a) *MUM image* $v = [272 \times 192]$

Algorithm:
Step1: Apply log-Gabor filter to CLAHE image
$x = CLAHE\ image\ \ and\ \ y = result\ of\ log - Gabor\ filter$
Step2: Determine the detail signal (d) of the image
The residual or detail signal is given by $= x \ominus y$.
Step3: Multiply the Gain value (γ) by the detail signal $(d \otimes \gamma)$
Step4: Determine the result of the MUM algorithm
The result of the MUM algorithm is obtained by the Equation (1): $v = y \oplus (d \otimes \gamma)$

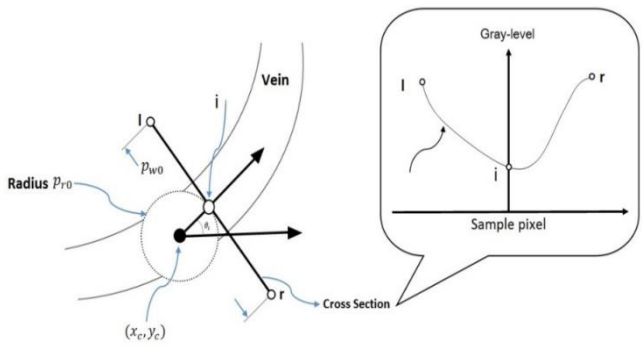

Figure 13: The relation of Current Tracking Point (CTP) on the cross-sectional profile [23]

The following equation is the line evaluation that detects the dark veins.

$$V_i = \max(x_i, y_i) \in N_c \{F(x_c + p_{r0}\cos\theta_i - {}^{p_{w0}}/_2 \sin\theta_i\ , y_c + p_{r0}\sin\theta_i + {}^{p_{w0}}/_2 \cos\theta_i) + F(x_c + p_{r0}\cos\theta_i + {}^{p_{w0}}/_2 \sin\theta_i\ , y_c + p_{r0}\sin\theta_i - {}^{p_{w0}}/_2 \cos\theta_i) - 2F(x_c + p_{r0}\cos\theta_i\ , y_c + p_{r0}\sin\theta_i)\} \quad (9)$$

Where the distance between the cross-sectional profile and the CTP is mentioned by r, the angle between line segments $(x_c, y_c) - (x_i, y_i)$ and $(x_c, y_c) - (x_c - 1, y_c)$ is shown by θ_i, p_{w0} is the width of profile, p_{r0} is the radius and (x_i, y_i) is the point at i. In this extraction algorithm, p_{w0} and p_{r0} are considered as 10 and 1, respectively.

$$\sin\ \theta_i = \frac{y_i - y_c}{[(x_i - x_c)^2 + (y_i - y_c)^2]^{1/2}} \quad (10)$$

$$\cos\ \theta_i = \frac{x_i - x_c}{[(x_i - x_c)^2 + (y_i - y_c)^2]^{1/2}} \quad (11)$$

The line tracking operates for all pixels of the image and the dark pixels of the image will be detected. The detection process of the entire pixels is repeated N times. The total number of times that each pixel of the input image is tracked as the dark point will be recorded. This dark point is termed as locus space. A higher number of elements of locus space is being repeatedly tracked indicating the higher probability of that location being the vein pixel.
In our case, the MUM algorithm can modify the sharpness and contrast of the image without any halo effect in the light region of the image [23]. The small and tiny veins in the enhanced image with the MUM algorithm are detectable, however, implementing the local contrast enhancement (CLAHE) at the initial stage before applying the MUM algorithm results in a more robust in-depth detection for the very tiny veins in the bright regions of the image. Thus better vein extraction is observed as shown in Figure 14.

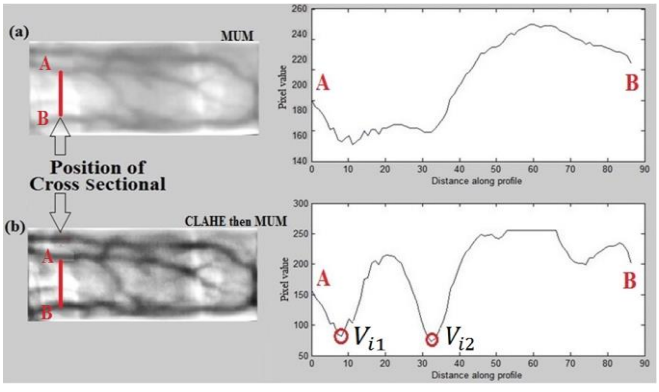

Figure 14: Cross-sectional profiles of the A-B line in MUM algorithm alone (a) and CLAHE before MUM algorithm applied (b)

Figure 14 shows the results of (a) MUM enhanced image and (b) proposed an enhanced image. From the observation, it is clear that both methods are viable in enhancing the sharpness of the images in the bright regions without any unpleasant halo effect. However, in terms of detection of the very tiny veins in the brightest part of the image, the CLAHE operator has shown significantly increased contrast of the tiny details. The advantage of the proposed method (CLAHE then MUM) can be observed by the cross-sectional profiles of a vertical line (A-B line) in the bright region as depicted in Figure 14. Here, the MRLT feature extraction algorithm works onto MUM enhancement image, which is not able to detect the depth of two branches of tiny veins in cross-sectional profile while the two valley shape points, V_{i1} and V_{i2} are able to be detected by the proposed enhanced algorithm (CLAHE then MUM). By using the local contrast enhancement method (CLAHE) before sharpness enhancement (MUM), the intensity of sharpness enhancement of the vein image was increased drastically and the tiny veins have become more detectable.

3. RESULTS AND DISCUSSION

In this section, the performances of extracted vein feature of the three different images: baseline image (without any modification), MUM enhancement image, and proposed enhancement method (CLAHE then MUM) image are validated. In this study, a Support Vector Machine (SVM) classifier was employed for the authentication of finger vein image [33].

3.1 Results of Image Enhancement and Feature Extraction

Figure 15 shows the baseline images, and the modified images by the MUM algorithm, and the proposed enhancement method (CLAHE and MUM) of an individual in the database. The index, ring, and middle fingers of both hands were captured for each subject in this database. As observed, the proposed enhancement technique can modify the contrast and sharpness of the finger image without any halo effect. Subsequently, the extracted vein pattern of the corresponding fingers is shown in Figure 16.

As observed, more details of tiny veins are detected in extracted vein feature using the proposed enhancement algorithm than compared to that of the baseline image extraction and MUM image extraction. Table 1 compares the number of white pixels (detected vein) for each extracted pattern of subjects that were shown in Figure 16.

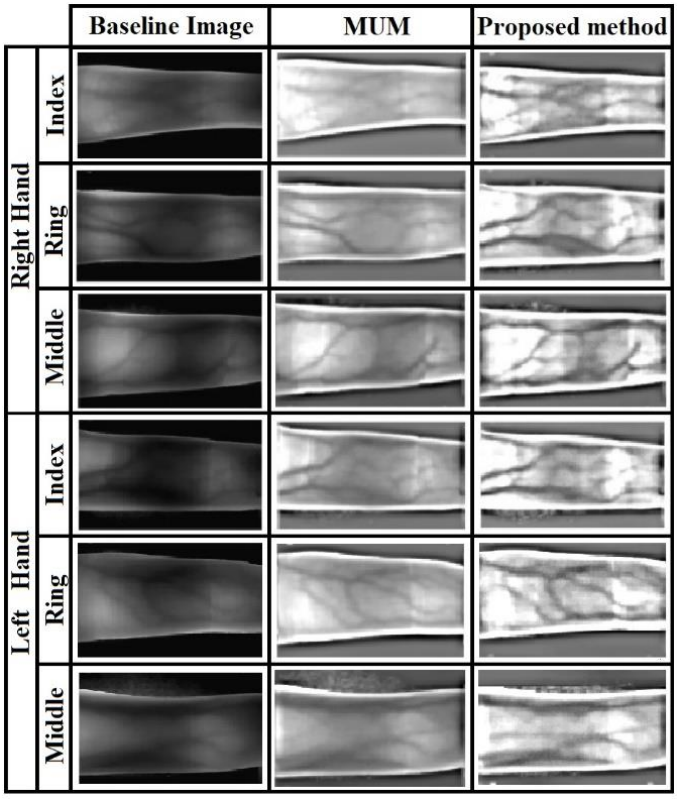

Figure 15: The baseline image, enhanced by MUM and proposed enhancement (CLAHE then MUM)

.

Table 1: Number of white pixels (extracted vein pattern) for each enhancement method

		Baseline Image	MUM	Proposed Enhancement
Right Hand	Index	575	712	921
	Ring	595	743	883
	Middle	503	828	999
Left Hand	Index	642	761	962
	Ring	629	801	1011
	Middle	512	820	987

3.2 Results of system performance

In this study, three ROC curves were plotted by GAR (Genuine Acceptance Rate) against the FAR (False Acceptance Rate) graph and the performances of the authentication system were evaluated for whole database according to the different numbers of training data with before and after image enhancement algorithm.

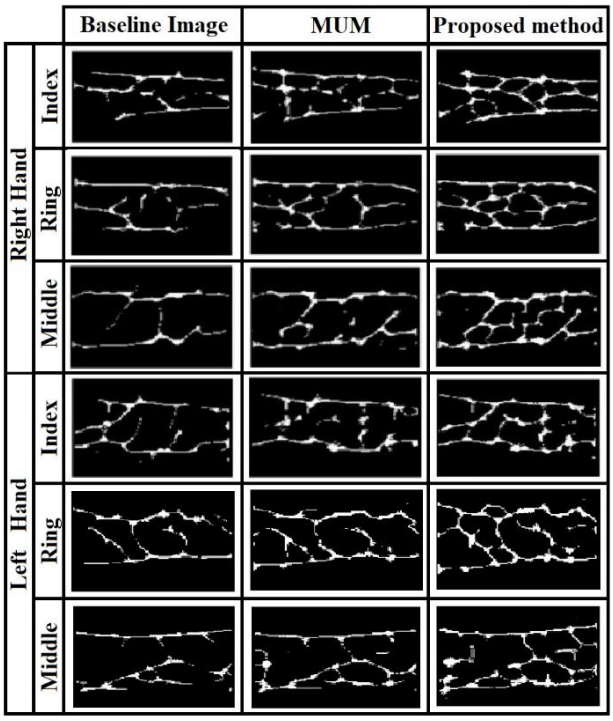

Figure 16: The extracted vein patterns of baseline images, and the images enhanced by MUM and proposed enhancement (CLAHE then MUM)

Figures 17, 18, and 19 show the performances of the authentication system based on one, two, and three training data, respectively. The baseline image (without any modification), the image enhanced by the MUM technique, and the image enhanced by the proposed algorithm are compared in these figures.

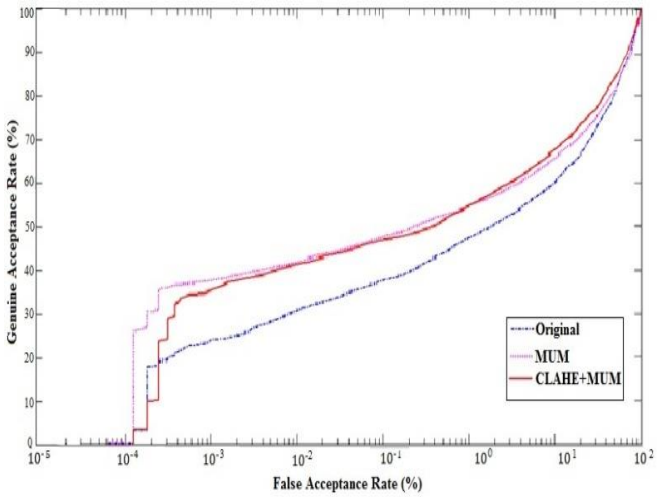

Figure 17: Performances of the system with different enhancement methods with one training data

Table 2: Genuine Acceptance Rates (GAR), Equal Error Rates (EER), and the number of images for each mode of data training according to the different types of image modification.

		Baseline		MUM		Proposed Method	
No. of Training	No. of Images	GAR (%)	EER (%)	GAR (%)	EER (%)	GAR (%)	EER (%)
1 to train 5 to test	636 3,180	47	26.63	54	26.39	56	23.32
2 to train 4 to test	1,272 2,544	53	26.64	63	21.59	70	16.82
3 to train 3 to test	1,908 1,908	68	16.66	78	9.22	92	6.28

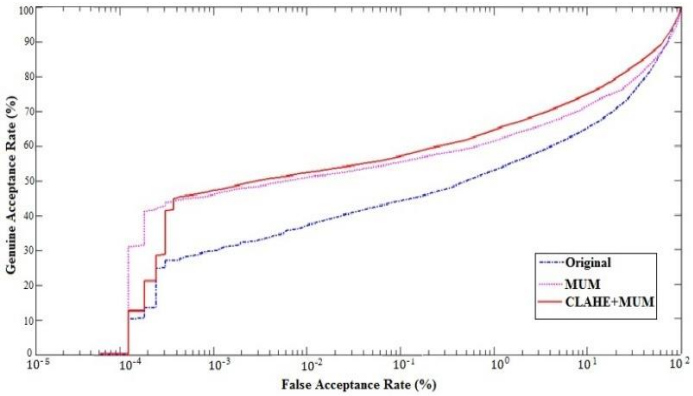

Figure 18: Performances of the system with different enhancement methods with two training data

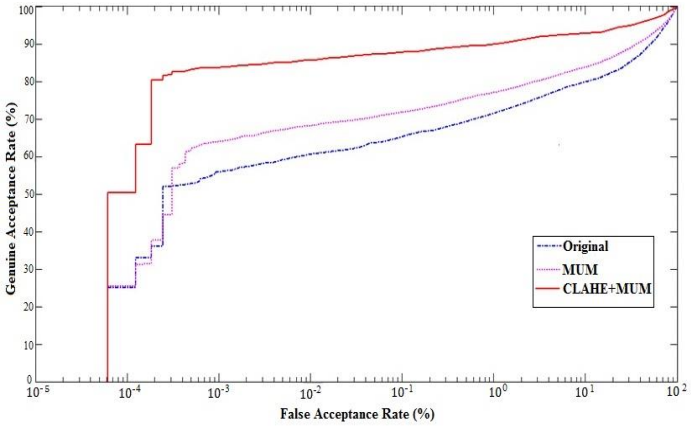

Figure 19: Performances of the system with different enhancement methods with three training data

By increasing the numbers of training data, the Genuine Acceptance Rate (GAR) of the system increases. The greatest GARs on one, two, and three data training are 56%, 70%, and 92%, respectively, which belong to the proposed image enhancement method. By increasing the numbers of training data, the Equal Error Rates (EERs) of the system decrease. The lowest EERs on one, two and three training data are 23.32%, 16.82%, and 6.28%, respectively, which also belong to the proposed image enhancement method. Table 2 shows the GARs, EERs, and the number of images used in each mode of training according to the types of image modifications.

The performance of Genuine Accuracy Rate (GAR) and Equal Error Rate based on three training data are 92% and 6.28%, respectively, which show a good improvement compared to Banerjee et al. (2018) and Hajian et al. (2018). The overall comparison results are illustrated in Table 3.

Table 3: Comparison with Previous Related Studies

Research studies	Database	Number of Individuals in Database	EER (%)	GAR (%)
Yang et al., (2009) [13]	Personal database	-	6.96	84
Yang et al., (2010) [14]	Personal database	70	10.04	78
Yang et al., (2014) [15]	Personal database	100	6	87
Banerjee et al., (2018) [17]	SDUML-HMT	106	9.43	88
Hajian et al., (2018) [23]	SDUML-HMT	106	9.22	79
Proposed method	SDUML-HMT	106	6.28	92

4. CONCLUSION

In this paper, the pre-processing stage in the finger vein authentication system has successfully been modified and evaluated. The Modified Repeated Line Tracking (MRLT), a robust finger vein feature extraction technique that operates based on image cross-sectional profile, was employed and the Support Vector Machine was used as a classifier for the authentication system. The proposed image modification technique significantly enhanced the sharpness and contrast of the finger image in such a way that small and tiny veins have become detectable by the MRLT processing method. The experimental results indicate that the importance of the CLAHE technique to be integrated with the MUM image enhancement approach in order to improve the contrast and sharpness of the finger vein image. Further investigation is warranted to improve the accuracy and performance of the finger vein verification system using more effective and robust valley detection approaches for feature extraction technique.

Acknowledgment

This research was sponsored and supported by a Research University (RU) Grant from Universiti Sains Malaysia (1001/PELECT/8014057).

REFERENCES

1. Syazana-Itqan, K., Syafeeza, A., and Saad, N. A review of finger-vein biometric identification approaches, Indian J of Sci. and Tech., **9**, 141-149, 2016.
2. Yang, W., Wang, S., Hu, J., Zheng, G., Valli, C. A fingerprint and finger-vein based cancellable multi-biometric system, Patt. Recog., **8**, 242-251, 2018.
3. Huang, Y. P., Luo, S. W., and Chen, E. Y. An efficient iris recognition system. *Inter. Conf. on Mach. Learn. and Cybernetics*, **1**, 450-454, 2002.
4. Tsai, W. Y., Barch, D. R., Cassidy, A. S., DeBole, M. V., Andreopoulos, A., Jackson, B. L., and Narayanan, V. Always-on speech recognition using true north, a reconfigurable, neurosynaptic processor. IEEE Trans. on Comp., **66**, 996-1007, 2016.
5. Kshirsagar, V. P., Baviskar, M. R., and Gaikwad, M. E. Face recognition using Eigenfaces. 3rd International Conference on Computer Research and Development, **2**, 302-306, 2011
6. Wen, X. B., and Liang, X. Z. Research on enhancing human finger vein pattern characteristics based on adjacent node threshold image method. Fifth Intern. Conf. on Frontier of Comp. Sci. and Tech., IEEE, 552-556, 2010.
7. Yang, L., Yang, G., Yin, Y., and Zhou, L. A survey of finger vein recognition. In Chinese Conf. on Biometric Recog., Springer, 234-243, 2014.
8. Huafeng, Q., Xiping , H., Xingyan, Y., and Hongbing, B. Finger-vein verification based on the curvature in Radon space. *Expert Sys. with Appl.*, ***82***, 151-161, 2017.
9. Kumar, T., Bhushan, S., and Jangra, S. A Brief Review of Image Quality Enhancement Techniques Based Multi-modal Biometric Fusion Systems. Intern. Conf. on Adv. Inform. for Comp. Research, 407-423, Singapore, 2018.
10. Ezhilmaran, D. and Rose Bindu Joseph, P. Fuzzy inference system for finger vein biometric images. Intern. Conf. on Inven. Sys. and Cont. (ICISC), IEEE, 1-4, 2017.
11. Miura, N., and Nagasaka, A. Feature extraction of finger-vein pattern based on repeated line tracking and its application to personal identification. Mach. Vis. and Appl., **15**, 194-203, 2004.
12. Hajian, A., and Ramli, D. A. A Study of Finger Vein Contrast Enhancement on Repeated Line Tracking Feature Extraction Method. 6th EEPC, Malaysia, 2016.
13. Yang, J., Yang, J., and Shi , Y. Finger-vein segmentation based on multi-channel even-symmetric gabor filters. Intern. Conf. on Intel. Comp. and Intell. Sys. (ICIS), **4**, 500-506, IEEE, 2009.
14. Yang, J., Yang, J., and Shi , Y. Combination of gabor wavelets and circular gabor filter for finger-vein extraction. Intern. Conf. on Intel. Comp. (ICIC), **57**, 346-354, 2010
15. Yang, J., and Shi, Y. Towards finger-vein image restoration and enhancement for finger-vein recognition. Inform. Sci. Informa. and Comp. Sci., Intelligent Systems, Applications, **268**, 33-52, 2014.
16. Banerjee, A., Basu, S., Basu, S., and Nasipuri, M. ARTeM: A new system for human authentication using finger vein images. Multimedia Tools and Appl., **77**, 5857-5884, 2018.
17. Gupta, P., and Gupta P. (2015). An accurate finger vein verification system. Dig. Sig. Proc., **38**, 43-52.

18. Yin, Y., Liu , L., and Sun , X. SDUMLA-HMT: A multimodal biometric database. Chinese Conf. on Comp. Sci. Biometric Recog. (CCBR), 260-268, 2011.
19. Das, R., Piciucco, E., Maiorana, E. and Campisi, P. Convolutional Neural Network for Finger-Vein-Based Biometric Identification, IEEE Trans. on Inform. Foren. and Secu., **14**, 360-373, 2018.
20. Kang, B. J., Park, K. R., Yoo, J. H., and Kim, J. N. Multimodal biometric method that combines veins, prints, and shape of a finger. Opti. Eng., **50**, 017201, 2011.
21. Yang, J., Wei, J., and Shi, Y. Accurate ROI Localization and Hierarchical Hyper-sphere Model for Finger-vein Recognition, Neurocomputing, **328**, 171-181, 2018.
22. Gurpreet, K. An enhancement of classical unsharp mask filter for contrast and edge preservation. Intern. J. of Eng. Sci. and Research Tech., ISSN, 2277-9655, 2013.
23. Hajian, A., and Ramli, D. A. Sharpness enhancement of finger-vein image based on modified un-sharp mask with log-Gabor filter. Procedia Comp. Sci., **126**, 431-440, 2018.
24. Marr, D. Vision: A computational investigation into the human representation and processing of visual information. MIT press, 1982.
25. Myers, D. G. Digital signal processing: efficient convolution and Fourier transforms techniques. Prentice-Hall, Inc., 1990.
26. Yu, C. H. Exploratory data analysis. Methods, **2**, 131-160, 1977.
27. Kumar, R., and Sharma, H. Comparative study of CLAHE, DSIHE and DHE schemes. Intern. J. of Research in Manag., Sci. and Tech., **1**, 1-4, 2008.
28. Gupta, S., and Kaur, y. Review of different local and global contrast enhancement techniques for a digital image. Intern. J. of Comp. Appl. (IJCA), **100**, 18-23, 2014.
29. Miura, N., Nagasaka, A., and Miyatake, T. Extraction of finger-vein patterns using maximum curvature points in image profiles. IEICE Trans. on Inform. and Sys., 1185-1194, **90**, 2007.
30. Hajian, A., and Damavandinejadmonfared, S. Optimal feature extraction dimension in finger vein recognition using Kernel Principal Component Analysis. Intern. J. of Comp., Inform., Sys. and con. Eng., **8**,1637-1640, 2014.
31. Yang, G., Xi, X., and Yin, Y. (2012). Finger vein recognition based on personalized best bit map. Sensors,**12**,1738–1757, 2012.
32. Liu, T., Xie , J., Yan , W., Li , P. Q., and Lu , H. Z. An algorithm for finger-vein segmentation based on modified repeated line tracking. The Imag. Sci. J., **61**, 491-502, 2013.
33. Ben-Yacoub, S., 1998. Multi-modal data fusion for person authentication using SVM (No. REP_WORK). IDIAP.